

Acoustic radiation force on a cylindrical composite particle with an elastic thin shell and an internal eccentric liquid column in a plane ultrasonic wave field

Rui-Qi Pan(潘瑞琪), Zhi-Wei Du(杜芷玮), Cheng-Hui Wang(王成会), Jing Hu(胡静), and Run-Yang Mo(莫润阳)
Citation: Chin. Phys. B, 2024, 33 (**9**): 094302. DOI: 10.1088/1674-1056/ad5d66
Journal homepage: http://cpb.iphy.ac.cn; http://iopscience.iop.org/cpb

What follows is a list of articles you may be interested in

Scheme of negative acoustic radiation force based on a multiple-layered spherical structure

Menyang Gong(宫门阳), Xin Xu(徐鑫), Yupei Qiao(乔玉配), Jiehui Liu(刘杰惠), Aijun He(何爱军), and Xiaozhou Liu(刘晓宙)
Chin. Phys. B, 2024, 33 (**1**): 014302. DOI: 10.1088/1674-1056/acfa80

Acoustic radiation force on a rigid cylinder near rigid corner boundaries exerted by a Gaussian beam field

Qin Chang(常钦), Yuchen Zang(臧雨宸), Weijun Lin(林伟军), Chang Su(苏畅), and Pengfei Wu(吴鹏飞)
Chin. Phys. B, 2022, 31 (**4**): 044302. DOI: 10.1088/1674-1056/ac2d1f

Rotational manipulation of massive particles in a 2D acoustofluidic chamber constituted by multiple nonlinear vibration sources

Qiang Tang(汤强), Pengzhan Liu(刘鹏展), and Shuai Tang(唐帅)
Chin. Phys. B, 2022, 31 (**4**): 044301. DOI: 10.1088/1674-1056/ac1f0e

Weak-focused acoustic vortex generated by a focused ring array of planar transducers and its application in large-scale rotational object manipulation

Yuzhi Li(李禹志), Peixia Li(李培霞), Ning Ding(丁宁), Gepu Guo(郭各朴), Qingyu Ma(马青玉), Juan Tu(屠娟), and Dong Zhang(章东)
Chin. Phys. B, 2021, 30 (**4**): 044302. DOI: 10.1088/1674-1056/abca1f

Axial acoustic radiation force on an elastic spherical shell near an impedance boundary for zero-order quasi-Bessel-Gauss beam

Yu-Chen Zang(臧雨宸), Wei-Jun Lin(林伟军), Chang Su(苏畅), and Peng-Fei Wu(吴鹏飞)
Chin. Phys. B, 2021, 30 (**4**): 044301. DOI: 10.1088/1674-1056/abca27

Acoustic radiation force on a cylindrical composite particle with an elastic thin shell and an internal eccentric liquid column in a plane ultrasonic wave field

Rui-Qi Pan(潘瑞琪), Zhi-Wei Du(杜芷玮), Cheng-Hui Wang(王成会)[†], Jing Hu(胡静)[‡], and Run-Yang Mo(莫润阳)

Institute of Shaanxi Key Laboratory of Ultrasonics, Shaanxi Normal University, Xi'an 710119, *China*

(Received 12 April 2024; revised manuscript received 14 June 2024; accepted manuscript online 1 July 2024)

A model with three-layer structure is introduced to explore the acoustic radiation force (ARF) on composite particles with an elastic thin shell. Combing acoustic scattering of cylinder and the thin-shell theorem, the ARF expression was derived, and the longitudinal and transverse components of the force and axial torque for an eccentric liquid-filled composite particle was obtained. It was found that many factors, such as medium properties, acoustic parameters, eccentricity, and radius ratio of the inner liquid column, affect the acoustic scattering field of the particle, which in turn changes the forces and torque. The acoustic response varies with the particle structures, so the resonance peaks of the force function and torque shift with the eccentricity and radii ratio of particle. The acoustic response of the particle is enhanced and exhibits higher force values due to the presence of the elastic thin shell and the coupling effect with the eccentricity of the internal liquid column. The decrease of the inner liquid density may suppress the high-order resonance peaks, and internal fluid column has less effects on the change in force on composite particle at $ka > 3$, while limited differences exist at $ka < 3$. The axial torque on particles due to geometric asymmetry is closely related to ka and the eccentricity. The distribution of positive and negative force and torque along the axis ka exhibits that composite particle can be manipulated or separated by ultrasound. Our theoretical analysis can provide support for the acoustic manipulation, sorting, and targeting of inhomogeneous particles.

Keywords: acoustic radiation force, acoustic scattering of cylinders, elastic shell, composite particles

PACS: 43.25.+y, 43.35.+d **DOI:** 10.1088/1674-1056/ad5d66

1. Introduction

Acoustic radiation force (ARF) has been extensively employed in the medical field during the past few decades,[1,2] including medical diagnosis and prediction,[3] cell manipulation,[4] delivery and release of targeted drugs,[5,6] and muscle therapy.[7] A common application of ARF is acoustic manipulation, where sound waves interact with target particles, through energy and momentum transfer to achieve acoustic manipulation. Acoustic manipulation is an important tool for doctors to diagnose and treat diseases.[8,9] Wu *et al.*[10] experimentally compared drug delivery efficiency with and without ultrasound and showed that using ultrasound does improve the efficiency of targeted drug delivery. Manipulation of cell is key to investigate treatments for various diseases. Yannapol *et al.*[11] utilized the structural vibration of a cylindrical glass tube to achieve rapid cell accumulation during bioprinting by acoustic manipulation, and found that neovascular network was enhanced by ultrasound, and experimentally verified that acoustic manipulation did not seriously damage cell activity. Yamaguchi *et al.*[12] employed ultrasound dual ARF to deform muscle tissue, and measured the displacement and strain produced by the muscle tissue using various ultrasound probes which provide noninvasive measurements to diagnose muscle conditions. Compared to other methods, acoustic manipulation can manipulate multiple particles simultaneously. Acoustic manipulation has the advantage of excellent biocompatibility, high efficiency, label-free, and noninvasiveness. Acoustic manipulation is emerging and promising to be explored in the future.

ARF is the fundamental of acoustic manipulation. Numerous researchers have investigated the ARF on particles, such as rigid and elastic cylinders, elastic cylinder shells, multiple-layered structure, etc.[13–19] Most papers on ARF have been focused on concentric models for cylinder and cylindrical shell.[20–24] On the other hand, analytical theories dealing with the problem of ARF acting on the eccentricity of a layered fluid inside a cylinder seems to be relatively few. In practical applications, the object of acoustic manipulation often involves inhomogeneous particles, leading many scholars have conducted extensive research on the effect of eccentricity on ARF. Shaw and Tai[25] used Helmholtz integral equation formula to obtain the analytical expression of ARF function generated by applying time-harmonic pressure at the inner boundary of eccentric composite cylinder in unbounded acoustic fluid. In order to derive analytical expressions for the scattered pressure field and each scattering cross-section for a cylinder with a hard or soft boundary inside a soft boundary, Roumeliotis *et al.*[26] used the translation addition theorem for

[†]Corresponding author. E-mail: wangld001@snnu.edu.cn
[‡]Corresponding author. E-mail: hjwlx@snnu.edu.cn

© 2024 Chinese Physical Society and IOP Publishing Ltd

cylindrical Bessel functions. Their results showed that the internal structure's location and acoustic properties can significantly alter the linear scattering of the cylinder. Danila *et al.*[27] calculated the equation for the scattered field at the interface of a plane wave incident on a cylindrical fluid shell using the generalized Debye series expansion to establish and analyze the gradient distribution equations for concentric and eccentric multilayered cylindrical fluid shells. Simao *et al.*[28] investigated the resonant scattering when the eccentric cylindrical position changed. Hasheminejad *et al.*[29,30] developed a model of an eccentric compound circular cylinder in an unbounded medium and derived the backscattered form function of the model considering viscoelastic. Based on this, the thermal viscosity of the medium is further considered to obtain the analytical expression for the ARF function of the eccentric fluid column. It is noted that the effect of thermal viscosity on the scattered field of the liquid column is typically amplified with increasing eccentricity. Mitri[31] analyzed the effect of centrifugal rate on the ARF and the axial torque of a layered liquid column, and it is pointed out that with the variation of parameters such as eccentricity and incidence angle, the transverse or longitudinal ARF arises on the compound cylinder. Due to the asymmetry of the model, the axial torque on the composite cylinder appears as a component, dimensional coefficients, eccentricity, and angle of incidence wave of the compound cylinder dictate the positive or negative value.

In most of the previous theoretical models, for inhomogeneous particles in membrane structures, the effect of elasticity of the shell on ARF has been neglected. For this purpose, a more realistic model needs to be developed to estimate the ARF of the target particle. Accordingly, we extended Mitri's model[31] and combined with Junger's theory[32] to research the ARF on a membrane structure, which consists by a composite elastic thin cylindrical shell subjected to a plane wave acoustic field. The ARF function of a composite cylindrical shell particle with an inner eccentric liquid column is derived. This investigation enriches the ARF theory, and helps to explore ultrasound technology in medical and engineering applications.

2. Theoretical model

A composite particle consists of liquid column encapsulated by a thin elastic cylindrical shell of thickness h and contained an eccentrical liquid column, as shown in Fig. 1. A plane wave is incident at arbitrary angle α. To facilitate the analysis, two sets of cylindrical coordinate systems (r_1, θ_1) and (r_2, θ_2) were established to analyze the ARF acting on composite fluid-filled particle, and the origins were at the center O_1 of the cylindrical shell and the center O_2 of the eccentric liquid column, respectively, with an eccentric distance d. Three regions were introduced to describe the problem: region I was the exterior of the thin cylindrical shell, region II was liquid chamber, and region III was the eccentric liquid column. The densities and sound speeds of the four parts are given as (ρ_1, c_1), (ρ_2, c_2), (ρ_3, c_3), (ρ_s, c_s), respectively.

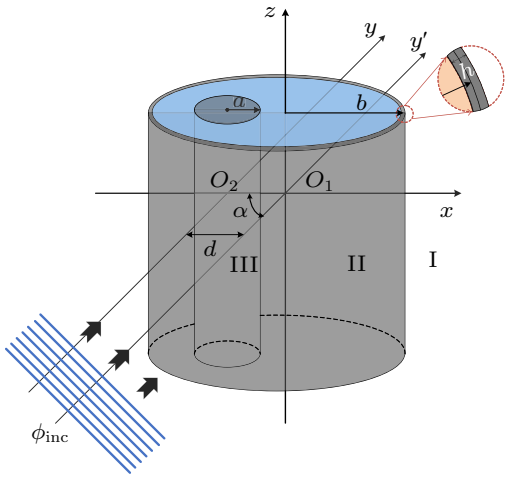


Fig. 1. Schematic diagram of the geometric model.

It is assumed that the external fluid medium is an ideal compressible and inviscid fluid. Using the partial-wave series expansion method in cylindrical coordinate, the incident plane wave and its scattered filed can be represented by the velocity potential as

$$\varphi_{\text{inc}} = \varphi_0 \mathrm{e}^{-\mathrm{i}\omega t} \sum_{n=-\infty}^{+\infty} \mathrm{i}^n \mathrm{e}^{-\mathrm{i}n\alpha} \mathrm{J}_n(k_1 r_1) \mathrm{e}^{\mathrm{i}n\theta_1}, \tag{1}$$

$$\varphi_{\text{sca}} = \varphi_0 \mathrm{e}^{-\mathrm{i}\omega t} \sum_{n=-\infty}^{+\infty} A_n \mathrm{H}_n^{(1)}(k_1 r_1) \mathrm{e}^{\mathrm{i}n\theta_1}, \tag{2}$$

where $\mathrm{J}_n(\cdot)$ is the cylindrical Bessel function of the first kind of order n, $\mathrm{H}_n^{(1)}(\cdot)$ is the cylindrical Hankel function of the first kind of order n with the coefficients A_n, $k_i = \omega/c_i$ $(i = 1, 2, 3)$ is the wavenumber in the medium of wave propagation. Therefore, the total sound field outside the elastic cylindrical shell is

$$\begin{aligned}\varphi_{\text{t}} = \varphi_0 \mathrm{e}^{-\mathrm{i}\omega t} \sum_{n=-\infty}^{+\infty} \big[&\mathrm{i}^n \mathrm{e}^{-\mathrm{i}n\alpha} \mathrm{J}_n(k_1 r_1) \\ &+ A_n \mathrm{H}_n^{(1)}(k_1 r_1)\big] \mathrm{e}^{\mathrm{i}n\theta_1}.\end{aligned} \tag{3}$$

Similarly, the velocity potential at II and III can be obtained as

$$\begin{aligned}\varphi_{t,\text{II}} = \varphi_0 \mathrm{e}^{-\mathrm{i}\omega t} \sum_{n=-\infty}^{+\infty} \big[&B_n \mathrm{J}_n(k_2 r_1) \mathrm{e}^{\mathrm{i}n\theta_1} \\ &+ C_n \mathrm{H}_n^{(1)}(k_2 r_2) \mathrm{e}^{\mathrm{i}n\theta_2}\big],\end{aligned} \tag{4}$$

$$\varphi_{t,\text{III}} = \varphi_0 \mathrm{e}^{-\mathrm{i}\omega t} \sum_{n=-\infty}^{+\infty} D_n \mathrm{J}_n(k_3 r_2) \mathrm{e}^{\mathrm{i}n\theta_2}. \tag{5}$$

In the cylinder coordinate system, the generalized radial and tangential displacement components associated with the thin

shell deformation are expanded with the Fourier series as follows:[32]

$$W_n = \sum_{n=0}^{\infty} a_n \mathrm{e}^{\mathrm{i}n\theta_1}, \tag{6}$$

$$V_n = -\mathrm{i}\sum_{n=1}^{\infty} b_n \mathrm{e}^{\mathrm{i}n\theta_1}, \tag{7}$$

The coefficients a_n and b_n satisfy the following equations of shell motion.[32] The coefficients a_n and b_n are the generalized coordinates of the system, must satisfy two sets of Lagrange equations which can be expressed as

$$\begin{aligned} &2h\rho_s\ddot{a}_n + \frac{2Eh}{(1-\nu^2)a^2}\left\{\left[1+\frac{n^4}{3}\left(\frac{h}{a}\right)^2\right]a_n\right. \\ &\left.+n\left[1+\frac{n^2}{3}\left(\frac{h}{a}\right)^2\right]b_n\right\} = -\mathrm{i}\omega\Delta\varphi, \\ &ah\rho_s\ddot{b}_n + \frac{nEh}{(1-\nu^2)a}\left\{\left[1+\frac{n^2}{3}\left(\frac{h}{a}\right)^2\right]a_n\right. \\ &\left.+n\left[1+\frac{1}{3}\left(\frac{h}{a}\right)^2\right]b_n\right\} = 0, \end{aligned} \tag{8}$$

$$\begin{aligned} \Delta\varphi &= \rho_2\left[B_n\mathrm{J}_n(k_2a_-)+\mathrm{H}_n^{(1)}(k_2a_-)\sum_{m=-\infty}^{\infty}C_m\mathrm{J}_{n-m}(k_2d)\right] \\ &+\rho_1\left[\mathrm{i}^n\mathrm{e}^{-\mathrm{i}n\alpha}\mathrm{J}_n(k_1a_+)+A_n\mathrm{H}_n^{(1)}(k_1a_+)\right], \end{aligned} \tag{9}$$

where ρ_s and E are density and Young's modulus of the elastic shell, with Poisson's ratio ν. Integrating Eqs. (8) and (9), it yields

$$a_n = -\Delta\varphi/Z_n, \tag{10}$$

$$b_n = \frac{n\left[1+\frac{n^2}{3}\left(\frac{h}{a}\right)^2\right]}{\omega^2a^2\rho_s(1-\upsilon^2)/E - n^2\left[1+\frac{1}{3}\left(\frac{h}{a}\right)^2\right]}a_n, \tag{11}$$

$$Z_n = 2\mathrm{i}\frac{h}{a}\left\{c_1\rho_s x - \frac{E}{c_1(1-\upsilon^2)x}\left[1+\frac{n^4}{3}\left(\frac{h}{a}\right)^2+\frac{n^2\left[1+\frac{n^2}{3}\left(\frac{h}{a}\right)^2\right]^2}{\omega^2a^2\rho_s(1-\upsilon^2)/E - n^2\left(1+\frac{1}{3}\left(\frac{h}{a}\right)^2\right)}\right]\right\}, \tag{12}$$

where $x = k_1a$, and the inner and outer radii of the shell are $a_+ = a + h/2$, $a_- = a - h/2$, respectively. Unknown coefficients A_n, B_n, C_n, D_n can be determined by the boundary conditions at the interfaces between regions I and II, and regions II and III. At the surface of the eccentric liquid column ($r_2 = b$), the acoustic pressure and velocity are continuous, with

$$\begin{aligned} &\mathrm{J}_n(k_2b)\sum_{m=-\infty}^{\infty}B_m\mathrm{J}_{m-n}(k_2d)+C_n\mathrm{H}_n^{(1)}(k_2b) \\ &= D_n\mathrm{J}_n(k_3b), \end{aligned} \tag{13}$$

$$\begin{aligned} &\mathrm{J}_n'(k_2b)\sum_{m=-\infty}^{\infty}B_m\mathrm{J}_{m-n}(k_2d)+C_n\mathrm{H}_n^{(1)'}(k_2b) \\ &= \frac{\rho_2c_2}{\rho_3c_3}D_n\mathrm{J}_n'(k_3b). \end{aligned} \tag{14}$$

The coupled equation gives a relationship between the coefficients B_n and C_n as

$$C_n = M_n\sum_{m=-\infty}^{\infty}B_m\mathrm{J}_{m-n}(k_2d), \tag{15}$$

$$M_n = \frac{\frac{\rho_3c_3}{\rho_2c_2}\mathrm{J}_n'(k_2b)\mathrm{J}_n(k_3b)-\mathrm{J}_n(k_2b)\mathrm{J}_n'(k_3b)}{\mathrm{J}_n'(k_3b)\mathrm{H}_n^{(1)}(k_2b)-\frac{\rho_3c_3}{\rho_2c_2}\mathrm{J}_n(k_3b)\mathrm{H}_n^{(1)'}(k_2b)}. \tag{16}$$

At $r_1 = a$, due to the radial velocity continuum at the inner and outer surfaces of the cylindrical shell, one has

$$\begin{aligned} &\frac{1}{c_1}\left[\mathrm{i}^n\mathrm{e}^{-\mathrm{i}n\alpha}\mathrm{J}_n'(k_1a_+)+A_n\mathrm{H}_n^{(1)'}(k_1a_+)\right] \\ &= \mathrm{i}\Delta\varphi/Z_n, \end{aligned} \tag{17}$$

$$\begin{aligned} &\frac{1}{c_2}\left[B_n\mathrm{J}_n'(k_2a_-)+\mathrm{H}_n^{(1)'}(k_2a_-)\sum_{m=-\infty}^{\infty}C_m\mathrm{J}_{n-m}(k_2d)\right] \\ &= \mathrm{i}\Delta\varphi/Z_n, \end{aligned} \tag{18}$$

Accordingly, the coupling relationship yields

$$\begin{aligned} &S_n + R_nA_n + \rho_2\mathrm{H}_n^{(1)}(k_2a_-)\sum_{m=0}^{\infty}M_m \\ &\times\left(\sum_{j=0}^{\infty}\frac{\eta_j\mathrm{i}^j\mathrm{e}^{-\mathrm{i}j\alpha}+\varsigma_jA_j}{d_j}\mathrm{J}_{j-m}(k_2d)\right)\mathrm{J}_{n-m}(k_2d) = 0, \end{aligned} \tag{19}$$

where

$$S_n = \left[\rho_2\mathrm{J}_n(k_2a_-)\frac{\eta_n}{d_n}-\frac{Z_n}{\mathrm{i}c_1}\mathrm{J}_n'(k_1a_+)+\rho_1\mathrm{J}_n(k_1a_+)\right]\mathrm{i}^n\mathrm{e}^{-\mathrm{i}n\alpha},$$

$$R_n = \rho_2\mathrm{J}_n(k_2a_-)\frac{\varsigma_n}{d_n} + \left[\rho_1\mathrm{H}_n^{(1)}(k_1a_+)-\frac{Z_n}{\mathrm{i}c_1}\mathrm{H}_n^{(1)'}(k_1a_+)\right],$$

$$\eta_n = \frac{\rho_2c_2}{c_1}\mathrm{J}_n'(k_1a_+)\mathrm{H}_n^{(1)}(k_2a_-)+\rho_1\mathrm{J}_n(k_1a_+)\mathrm{H}_n^{(1)'}(k_2a_-) - \frac{Z_n}{\mathrm{i}c_1}\mathrm{J}_n'(k_1a_+)\mathrm{H}_n^{(1)'}(k_2a_-),$$

$$\varsigma_n = \frac{\rho_2c_2}{c_1}\mathrm{H}_n^{(1)'}(k_1a_+)\mathrm{H}_n^{(1)}(k_2a_-) + \rho_1\mathrm{H}_n^{(1)}(k_1a_+)\mathrm{H}_n^{(1)'}(k_2a_-) - \frac{Z_n}{\mathrm{i}c_1}\mathrm{H}_n^{(1)'}(k_1a_+)\mathrm{H}_n^{(1)'}(k_2a_-),$$

$$d_n = \rho_2 \left[\mathrm{J}_n'(k_2 a_-)\mathrm{H}_n^{(1)}(k_2 a_-) - \mathrm{J}_n(k_2 a_-)\mathrm{H}_n^{(1)'}(k_2 a_-) \right].$$

Solving Eq. (20), the scattering coefficients A_n of the compound particle can be obtained. In the solution process, the coefficients are determined by solving a system of linear equations after taking a truncation value n.[33]

3. Acoustic radiation force

In an unbounded ideal liquid, the ARF acting on a cylinder in a plane waves acoustic field is often expressed as the surface integral of the time-averaged value of the additional pressure, which is related to the nonlinear perturbation formed by the acoustic wave in the medium, i.e., the ARF function of the elastic cylindrical shell is[34]

$$\langle \boldsymbol{F} \rangle \underset{k_1 r_1 \to \infty}{=} \frac{1}{2}\rho_1 k_1^2 \int_0^{2\pi} \mathrm{Re}\{\Phi_{is}(r_1,\theta_1,t)\}\,\mathrm{d}\boldsymbol{S}, \tag{21}$$

where $\mathrm{Re}\{\cdot\}$ denotes the real part of the total velocity potential of region I, $\mathrm{d}\boldsymbol{S} = \mathrm{d}S\boldsymbol{e_r}$, $\boldsymbol{e_r}$ is the radial unit vector at the cylinder surface element $\mathrm{d}S$. It can be obtained that $\boldsymbol{e_r}$ satisfies $\boldsymbol{e_r} = \cos\theta \boldsymbol{e_x} + \sin\theta \boldsymbol{e_y}$ with the x-axis and y-axis unit vectors,

$$\begin{aligned} &\Phi_{is}(r_1,\theta_1,t) \\ &\underset{k_1 r_1 \to \infty}{=} \varphi_{\mathrm{sca}}^* \left[(\mathrm{i}/k_1)(\partial\varphi_{\mathrm{inc}}/\partial r_1) - \varphi_{\mathrm{inc}} - \varphi_{\mathrm{sca}} \right], \end{aligned} \tag{22}$$

where the superscript $*$ denotes the conjugate complex. The ARF along the x axis and y axis components can be expressed as[34]

$$\begin{Bmatrix} F_x \\ F_y \end{Bmatrix} = \langle \boldsymbol{F} \rangle \cdot \begin{Bmatrix} e_x \\ e_y \end{Bmatrix} = \begin{Bmatrix} Y_x \\ Y_y \end{Bmatrix} S_{\mathrm{c}} E_0, \tag{23}$$

where $E_0 = \frac{1}{2}\rho_1 k_1^2 |\varphi_0|^2$ is the average energy density of the incident plane wave, $S_{\mathrm{c}} = 2aL$ is the cross-sectional area per unit length of the cylinder, and one has

$$\int_0^{2\pi} \mathrm{e}^{\mathrm{i}(n'-n)\theta} \begin{Bmatrix} \cos\theta \\ \sin\theta \end{Bmatrix} \mathrm{d}\theta = \pi \begin{Bmatrix} (\delta_{n,n+1} + \delta_{n,n-1}) \\ \mathrm{i}\,(\delta_{n,n+1} - \delta_{n,n-1}) \end{Bmatrix}. \tag{24}$$

Substituting Eq. (22) into Eq. (21) and incorporating Eqs. (23) and (24), the dimensionless transverse and longitudinal ARF (Y_x and Y_y) yield

$$Y_x = \frac{1}{k_1 a}\,\mathrm{Im}\left\{ \sum_{n=-\infty}^{+\infty} \left(\mathrm{i}^n \mathrm{e}^{-\mathrm{i}n\alpha} + A_n \right) \left(A_{n+1}^* - A_{n-1}^* \right) \right\}, \tag{25}$$

$$Y_y = -\frac{1}{k_1 a}\,\mathrm{Re}\left\{ \sum_{n=-\infty}^{+\infty} \left(\mathrm{i}^n \mathrm{e}^{-\mathrm{i}n\alpha} + A_n \right) \left(A_{n+1}^* + A_{n-1}^* \right) \right\}, \tag{26}$$

where $\mathrm{Im}\{\cdot\}$ denote the imaginary part. The ARF function can be calculated by substituting the scattering coefficient A_n into Eqs. (25) and (26). The ARF is only related to the scattering coefficient A_n and $k_1 a$, which depends on the acoustic properties of the cylindrical shell medium, the inner liquid, and the eccentric liquid column.

The acoustic radiation torque function is[31]

$$\langle \boldsymbol{N} \rangle \underset{k_1 r_1 \to \infty}{=} -\rho_1 \iint_S \langle \boldsymbol{v} \otimes (r_1 \times \boldsymbol{v}) \rangle \cdot \mathrm{d}\boldsymbol{S}, \tag{27}$$

where $\otimes$ is the tensor product, $\boldsymbol{v} = \mathrm{Re}\{\nabla\varphi_t\}$. The z-axis time-averaged radiated torque vector component can be written as

$$N_z = \langle \boldsymbol{N} \rangle \cdot e_z = \frac{\rho_1}{2}\,\mathrm{Im}\left\{ \int_0^{2\pi} (\partial\varphi_t^*/\partial r_1)\hat{L}_z \varphi_t\,\mathrm{d}\boldsymbol{S} \right\}, \tag{28}$$

where e_z is the z-axis unit vector, $\hat{L}_z = -\mathrm{i}\partial/\partial\theta_1$ is the z-axis component of the angular momentum operator in the polar coordinate system. Integration of Eq. (28) yields an expression for the axial component of the radial torque vector as

$$N_z = \tau_z V E_0, \tag{29}$$

where $V = \pi a^2 L$ is the unit volume, and τ_z, the z-axis dimensionless radial torque function, is expressed as[31]

$$\tau_z = -\frac{4}{\pi (k_1 a)^2}\,\mathrm{Re}\left\{ \sum_{n=-\infty}^{+\infty} n \left(\mathrm{i}^n \mathrm{e}^{-\mathrm{i}n\alpha} + A_n \right) A_n^* \right\}. \tag{30}$$

Numerical analysis of the model by programming the solution equation and combining it with the relevant parameters.

4. Numerical analysis

Manipulating inhomogeneous particles is significantly more common in actuality. Numerical calculations were done via Eqs. (25), (26), and (30) to analyze the effects of particle structure and medium properties on the ARF of composite particles in a plane wave sound field, extending the basic theory of the thin-shell-encapsulated inhomogeneous particles for acoustic manipulation applications. For the numerical study, a stainless steel layered composite liquid column and a composite structure modeled on muscle tissue and cellular structure were chosen, and the parameters are presented in Appendix A.

4.1. Liquid particles with a stainless-steel cylindrical shell

To validate the model, in this paper, stainless steel thin shell material is adopted, with the external fluid being water, region II being filled with mercury, and the medium at the liquid column in region III being water, with reference to Mitri's model[31] which is illustrated in Figs. 2(a) and 2(b). The two-dimensional plots of transverse and longitudinal ARF with ka and incident angle α when the inner liquid column is located at the center of the cylindrical shell, i.e., $kd = 0$, $kb = 0.1$, are given in Figs. 2(c) and 2(d) (For clarity, k denotes k_1 in the following text). Obviously, the ARF exerted on the composite particles changes when the inner liquid is wrapped by the elastic thin cylindrical shell. By comparing with Mitri's results, it can be seen that the distribution of Y_x and Y_y with incidence angle is similar in character, and the peak position and magnitude vary significantly with the ka distribution. Due to the

acoustic response of the elastic thin shell, the acoustic scattering of the elastic thin cylindrical shell is significantly enhanced compared to that of the shell-less liquid column. The peaks of the Y_x plot of the composite cylindrical shell correspond to the ka value, and the main resonance peak appears at $ka = 3.3$. It is obvious that the existence of an elastic thin shell can modify the acoustic response of the composite cylinder. The difference of the ARF between shell-less and shelled cylinders results from the fact that the incident wave excites the forced vibrations of the thin shell, and the scattering mode is partly controlled by these vibrations. The resonant scattering of the liquid particle can be promoted by the elastic shell, which affects the ARF distribution too. Positive Y_y is symmetrically distributed along the axis of the incidence angle of 90°, while Y_x is negative for incidence angles greater than 90°, which means that the direction of the force acting on the object can be determined by the incidence angle of acoustic wave.

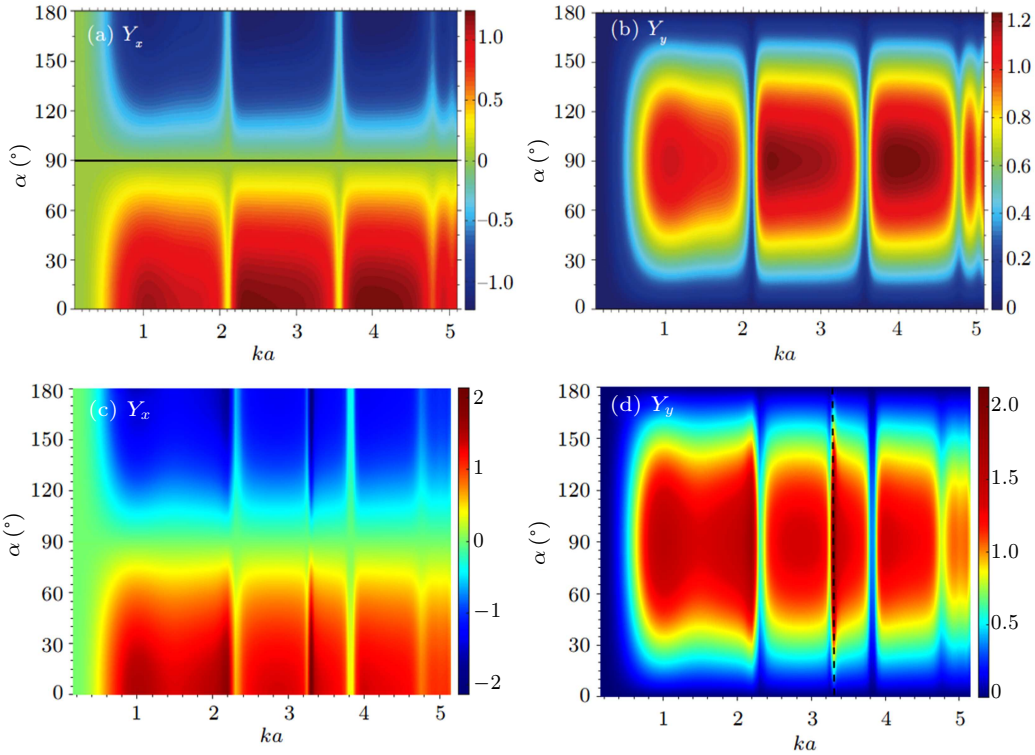


Fig. 2. The maps of components Y_x and Y_y in ka–α plane for a compound liquid particle with a stainless-steel elastic shell. Panels (a) and (c) transverse component Y_x, panels (b) and (d) are longitudinal component Y_y (panels (a) and (b) reprinted from Ref. [31]).

The ratio of the radius of the liquid column to the cylinder shell, b/a, is set as 0.3 to explore the impact of the position of the liquid column inside the shell on the ARF, as shown in Fig. 3. The Y_x curves are presented for different dimensionless d/a values of 0, 0.1, 0.3, 0.5, and 0.6, respectively, and it is found that there are many resonance peaks. The position of the liquid column significantly affects the response of composite particle. When the liquid column is located at the center, there is no obvious main resonance peak on the Y_x curve, while when the liquid column in the shell deviates from the center, the main resonance peak appears. The number of resonance peaks increases with increasing eccentricity, and the main resonance enhances, which indicates that the acoustic response of eccentric particles may be strengthened in a particular range of ka. Therefore, the eccentricity of the liquid column shows a significant effect on the acoustic distribution. It is possible to manipulate and separate particles based on their eccentricity rather than just relying on parameters such as their size. At the same time, the variation of the ARF property reflects the internal structure to a certain extent, which helps to obtain parameters such as the asymmetry of the internal structure.

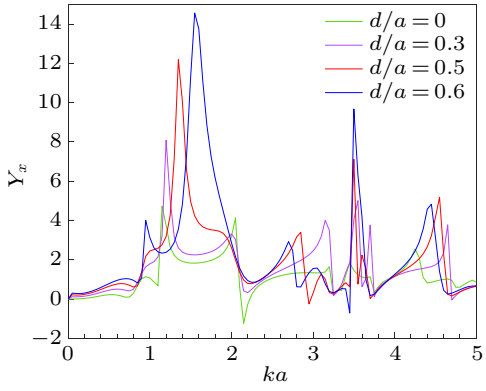


Fig. 3. The Y_x component of the ARF on a composite cylindrical liquid particle for different eccentricities ($d/a = 0$, 0.1, 0.3, 0.5, 0.6).

Fixing the angle of incidence at 0°, figure 4 gives the curves of ARF for relative eccentricity $d/a = 0$ and 0.3, respectively. The dimensionless shell thicknesses h/a equals 0, 0.01, 0.03, and 0.05, respectively. By comparing Figs. 4(a)

and 4(b), it can be seen that the ARF of the cylinder without shell is weaker than that of the liquid column encapsulated by the elastic shell, and it is obvious that the presence of the shell enhances the acoustic response of the composite particles, and the ARF curves appear to be bifurcated. In Fig. 4(a), the peak value of the main resonance of the shelled composite particles is minimized at the relative thickness of the shell layer $h/a = 0.05$. In contrast, in Fig. 4(b), the peak value of the main resonance of the composite particles is maximized at $h/a = 0.05$. The peak positions on ARF curves are slightly shifted, which indicates that this change in shell thickness results in less influence on the resonant frequency, rather than the acoustic response amplitude. As ka continues to increase, a large number of sharp peaks appear on the ARF curves, and the effect of thin shell thickness decreases. This may be related to the coupling effect of the acoustic wave-induced structural response, i.e., the acoustic response pattern of the shelled layers is different. It should be noted that the effect of shear waves in the elastic shell is neglected due to the thin shell theory. Therefore, it may lead to incorrect results when the shell thickness is large. Therefore, we chose the relative shell thickness of 0.01 for the numerical calculation.[32]

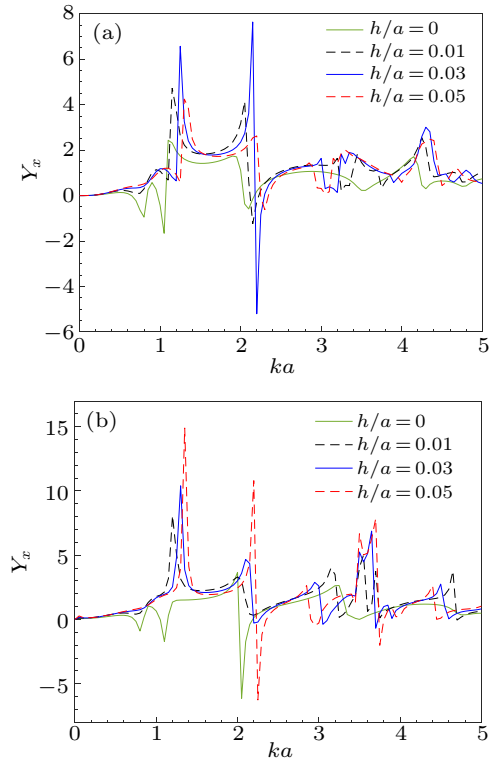


Fig. 4. Comparisons of the Y_x component on composite cylindrical particle: (a) concentric or (b) eccentric structures.

4.2. Muscle tissue model

Muscle tissue edema is a common tissue lesion, which attracted the attention of many researchers.[35] Based on the monitoring of muscle tissue edema, we used an elastic thin cylindrical shell to simulate the extra muscular membrane wrapping the myotubes, with the external liquid environment as water, region II as muscle tissue, and the eccentric liquid column medium as water. The ARF acting on the muscle tissue are investigated in the plane-wave acoustic field. For the composite structures with concentric liquid column and $b/a = 0.5$, the effects of the density of the medium on the ARF are calculated, as shown in Fig. 5. It can be observed that intracavity density affects the magnitude of resonance peak in the range of $ka < 1$, and for the case that the density is close to that of water, highest peak magnitude can be obtained. At $ka > 1$, weak fluctuation of the ARF can be observed, and the amplitude is suppressed with the increasing of the density of muscle tissue (Fig. 5(a)). The ARF is affect less by the density of inner liquid column, and it is found that there are small deviations of the fluctuation amplitude in the range of $ka < 3$. Therefore, the tissue should be the key factor to affect the acoustic response of the composite structure of muscle. The impedance gradient can intensify the scattering of the structure, therefore, the properties of the medium of the composite structure should be detected when ultrasound is used to relieve or treat tissue diseases, such as muscle edema.

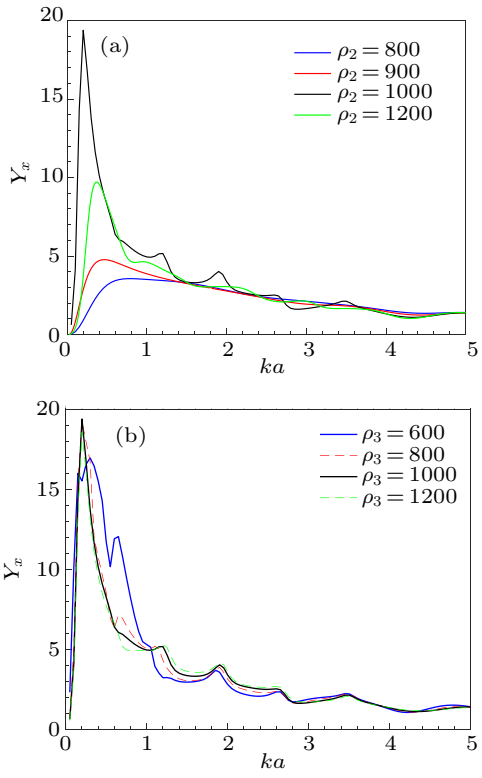


Fig. 5. The variation of Y_x components with density of medium in composite cylindrical shell: (a) medium in region II and (b) liquid in region III.

It is observed that if the structure is symmetrical, the torque equals 0, and the composite structure does not torsion, as shown in Fig. 6(a). For the case of eccentric composite structure with $b/a = 0.3$ and $d/a = 0.3$, it is found that axial torque is produced due to the disruption of the structural symmetry. The distribution of the torque is closely related to

the structural symmetry, and the critical incident angle equals 90° for reversal of torque direction. A strong torque appears around $ka = 1$ and $ka \ll 0$. The negative or positive torque should be related to the asymmetry of the structure. The uniformity of the tissue is damaged if local lesions occur, so it makes sense to analyze the acoustic torque exerted on non-uniform tissues for treating tissues with ultrasound. The amplitude of the torque varies with the incident angle, acoustic frequency, and the size of the myotubes. Actually, the alignment of muscle fibers can directly affect the function of skeletal muscle.[36] Therefore, it is worth noting that the frequency and incidence direction of the ultrasound should be set appropriately for different parts of muscle tissue to achieve a good therapeutic effect.

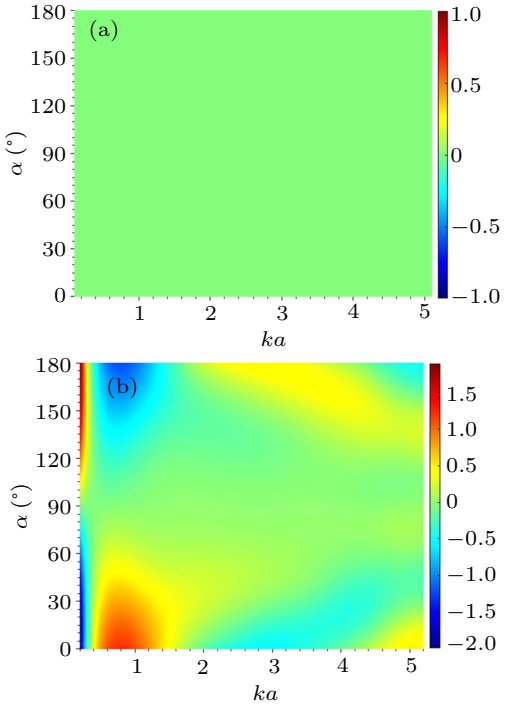


Fig. 6. Acoustic radiation torque on composite structure: (a) concentric and (b) eccentric ($d/a = 0.3$) cylindrical structures.

4.3. Schwann cell model

Cells can be isolated via contactless manipulation to help treat and monitor various diseases in the medical process.[37] Schwann cells can be considered as a typical inhomogeneous cylinder composite particle, whose manipulation is important for the ultrasonic nerve stimulation.[38] The nucleus of mature Schwann cells is off-center and close to the cell membrane, whereas the nucleus of immature Schwann cells is situated in the middle of the cell.[39] The surrounding fluid environment may have significant impacts on the manipulation of this cell, so water, glycerol and mercury were chosen here, as shown in Fig. 7. It is found that strong resonance responses of the ARF exerted on composite particles appears in the range of $ka < 1$ (Fig. 7(a)). For the case of water, whose impedance is close to that of inner liquid, the cell nucleus might have more effects on nonlinear energy in the scattering field when $ka \sim 0.1$, which means that the parameters should be optimized by size and structure of particle as well as surrounding fluid. The Y_x curve becomes flatten in Fig. 7(b), and several resonance peaks and fluctuations are observed in Fig. 7(c) when $ka > 1$, indicating that the ARF on particles in glycerol is more stable, and harmonic frequency resonance responses exist. Therefore, surrounding medium can affect the stability of the manipulation. For instance, some glycerol can be added to the surrounding medium to improve the manipulation stability when manipulating the composite particles with sound waves.

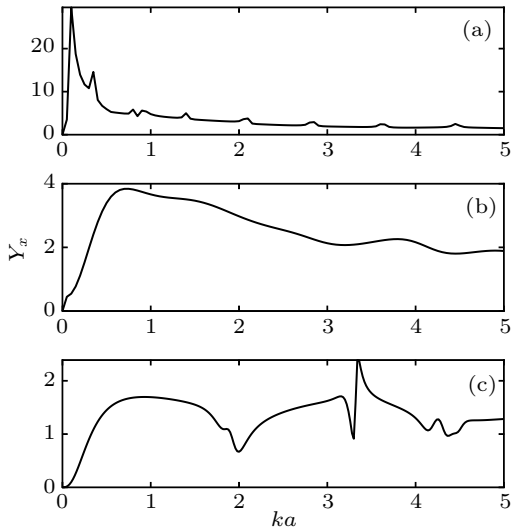


Fig. 7. The Y_x components of the ARF on cells suspended in different fluids: (a) water, (b) glycerol, and (c) mercury.

The impact of acoustic frequency on the manipulation of a suspending particle should be very distinctive, especially in the high-frequency region. The map of ARF at incident angle and particle size plane for driving frequencies of 1 MHz and 3 MHz, as shown in Fig. 8. In these figures, the radius ratio $b/a = 0.3$, and relative eccentricity $d/a = 0.3$. Referring to the experimental data of Sriphutkiat *et al.*,[11] the size of suspending cell is distributed in the range of 3 μm–10 μm. When the incident wave frequency is 1 MHz, the composite particles whose radii in the range of 6.4 μm–6.6 μm are obviously subjected to a stronger ARF, and another local peak appears at about 8.9 μm. The ARF is very sensitive to the particle size. The positive ARF are distributed in two narrow band, therefore, the certain size of the particles can be isolated. The incident angle of the wave mainly affects the fluctuations in the strong ARF distribution region, and has less influence on other regions. Similar trend is observed at 3-MHz frequency. However, the distribution region of positive ARF is wider, with a narrow negative force band at $a = 3.2$ μm.

The shape of cells is important in regulating their growth and functions,[40] and the inner structure may vary with the surrounding environment. For comparing the impacts of the structure, different radii ratios $b/a = 0.3$ and 0.6 are set to an-

alyze the acoustic torque exerted on the particles with eccentric ratios $d/a = 0.3$, as shown in Fig. 9. According to the two maps, it is found that the distribution of the torque is closely related with the radii ratio, which determines the resonance response of the particle to acoustic excitation. A strong response region can be observed at $ka < 0.85$ and $30° < \alpha < 150°$, along with many regions with different colors representing different magnitudes and directions. Therefore, composite particles can be driven to rotate counterclockwise or clockwise by ultrasound of appropriate frequency and incident direction.

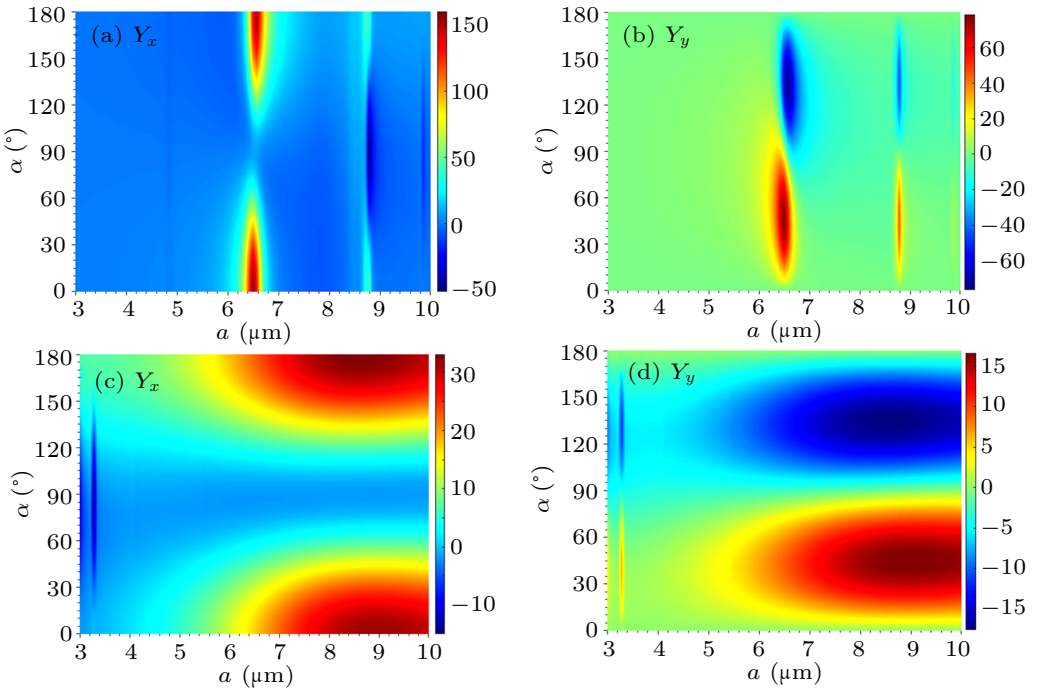


Fig. 8. Maps of components Y_x, Y_y of the force function in α–a plane. Acoustic frequencies [(a), (b)] $f = 1$ MHz, and [(c), (d)] 3 MHz.

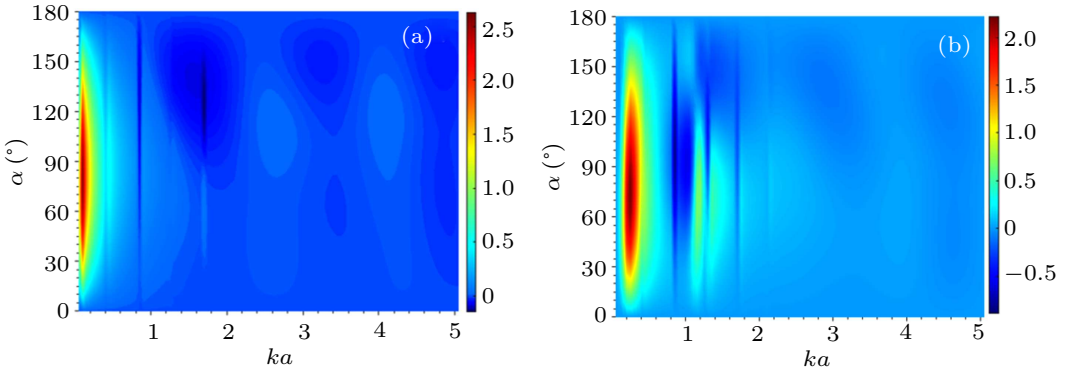


Fig. 9. Acoustic radiation torque on composite cylindrical particle with (a) $b/a = 0.3$ and (b) $b/a = 0.6$.

5. Discussion and conclusion

In this paper, a cylindrical composite structure of an elastic thin shell with an eccentric liquid column is proposed to analyze the ARF on particles with non-homogeneous mass distribution. By combining the thin-shell theory, the expressions of ARF and axial torque acting on the composite particle suspending in a liquid under the action of a plane acoustic field is derived. Three shell models, e.g., liquid column with a stainless steel cylindrical shell, muscle tissue, Schwann cell, are researched. Many factors, such as the thickness of elastic shell, incident direction of plane waves, eccentric rate of inner liquid column, and surrounding liquid, are considered. It is found that the broken symmetry of composite particles results in the axial torque. There are some key factors to affect the acoustic manipulation of composite particles, such as the acoustic frequency, density, and structure. Reasonable parameter selection can achieve effective manipulation and separation of particles.

Appendix A: Parameter of the model

The sound speed, density and impedance of the medium used in the numerical calculation are shown in Table A1, and the density, Young's modulus, and Poisson's ratio of the elastic cylindrical shell are shown in Table A2.[31,41,42]

Table A1. Parameters of liquid medium.

	Cell cytoplasm	Cell nucleus	Water	Mercury	Glycerol	Muscle tissue
Velocity (m/s)	1508	1508.5	1500	1407	1923	1600
Mass density (kg/m^3)	1000	1430	1000	13600	1260	1060
Impedance (MRayl)	1.51	2.16	1.5	19.1	2.42	1.70

Table A2. Some parameters of elastic shell.

Shell material	Mass density ρ (kg/m^3)	Young's modulus E	Poisson's ratio υ
Chitosan shell	600	200 MPa	0.4
Stainless steels	7900	200 GPa	0.264
Muscle	1060	0.79 MPa	0.4

Acknowledgements

Project supported by the National Natural Science Foundation of China (Grant Nos. 12374441 and 11974232) and the Fund from Yulin Science and Technology Bureau (Grant No. CXY-2022-178).

References

[1] Carugo D, Ankrett D N, Glynne-Jones P, Capretto L, Boltryk R J, Zhang X, Townsend P A and Hill M 2011 *Biomicrofluidics* **5** 044108
[2] Mittelstein D R, Ye J, Schibber E F, Roychoudhury A, Martinez L T, Fekrazad M H, Ortiz M, Lee P P, Shapiro M G and Gharib M 2020 *Appl. Phys. Lett.* **116** 013701
[3] Alan B, Utangaç M, Göya C and Dağgülli M 2016 *Med. Sci. Monit.* **22** 4523
[4] Li P, Mao Z, Peng Z, Zhou L, Chen Y, Huang P H, Truica C I, Drabick J J, El-Deiry W S, Suresh S and Huang T J 2015 *Proc. Natl. Acad. Sci. USA* **112** 4970
[5] Kopechek J A, McTiernan C F, Chen X, Zhu J, Mburu M, Feroze R, Whitehurst D A, Lavery L, Cyriac J and Villanueva F S 2019 *Theranostics* **9** 7088
[6] Lum A F H, Borden M A, Dayton P A, Kruse D E, Simon S I and Ferrara K W 2006 *Journal of Controlled Release* **111** 128
[7] Sánchez M, Anitua E, Delgado D, Prado R, Sánchez P, Fiz N, Guadilla J, Azofra J, Pompei O, Orive G, Ortega M, Yoshioka T and Padilla S 2015 *J. Tissue. Eng. Regener. Med.* **11** 1619
[8] Rapoport N, Kennedy A M, Shea J E, Scaife C L and Nam K H 2010 *Mol. Pharm.* **7** 22
[9] Meng L, Cai F, Li F, Zhou W, Niu L and Zheng H 2019 *J. Phys. D: Appl. Phys.* **52** 273001
[10] Zhang R, Guo H, Deng W, Huang X, Li F, Lu J and Liu Z 2020 *Appl. Phys. Lett.* **116** 123503
[11] Sriphutkiat Y, Kasetsirikul S, Ketpun D and Zhou Y 2019 *Sci. Rep.* **9** 17774
[12] Yamaguchi J, Hasegawa H and Kanai H 2012 *J. Med. Ultrasonics* **39** 279
[13] Wu J, Du G, Work S S and Warshaw D M 1990 *J. Acoust. Soc. Am.* **87** 581
[14] Hasegawa T, Saka K, Inoue N and Matsuzawa K 1988 *J. Acoust. Soc. Am.* **83** 1770
[15] Hasegawa T, Hino Y, Annou A, Noda H, Kato M and Inoue N 1993 *J. Acoust. Soc. Am.* **93** 154
[16] Qiao Y, Zhang X, Gong M, Wang H and Liu X 2020 *J. Appl. Phys.* **128** 044902
[17] Mitri F G 2015 *Ultrasonics* **62** 244
[18] Sharma G S, Marsick A, Maxit L, Skvortsov A, MacGillivray I and Kessissoglou N 2021 *J. Acoust. Soc. Am.* **150** 4308
[19] Gong M, Xu X, Qiao Y, Liu J, He A and Liu X 2024 *Chin. Phys. B* **33** 014302
[20] Janele P J, Mioduchowski A and Haddow J B 1991 *Int. J. Engng Sci.* **29** 1585
[21] Laulagnet B and Guyader J L 1994 *J. Acoust. Soc. Am.* **96** 277
[22] Jamali J, Naei M H, Honarvar F and Rajabi M 2011 *Journal of Mechanics* **27** 227
[23] Ilinskii Y A, Zabolotskaya E A, Hay T A and Hamilton M F 2012 *J. Acoust. Soc. Am.* **132** 1346
[24] Cai L W 2004 *J. Acoust. Soc. Am.* **115** 986
[25] Shaw R P and Tai G 1974 *J. Acoust. Soc. Am.* **56** 1437
[26] Roumeliotis J A and Kakogiannos N B 1995 *J. Acoust. Soc. Am.* **97** 2074
[27] Danila E B, Conoir J M and Izbicki J L 1995 *J. Acoust. Soc. Am.* **98** 3326
[28] Simao A G, Guimaraes L G and de Mendonça J P R F 1999 *Opt. Commun.* **170** 137
[29] Hasheminejad S M and Kazemirad S 2008 *J. Sound. Vib.* **318** 506
[30] Hasheminejad S M and Alibakhshi M A 2008 *Journal of Zhejiang University: Science A* **9** 65
[31] Mitri F G 2020 *Chin. Phys. B* **29** 114302
[32] Junger M C 1952 *J. Acoust. Soc. Am.* **24** 366
[33] Wiscombe W J 1980 *Appl. Opt.* **19** 1505
[34] Chang Q, Zang Y, Lin W, Su C and Wu P 2022 *Chin. Phys. B* **31** 044302
[35] Topchyan A, Tatarinov A, Sarvazyan N and Sarvazyan A 2006 *Ultrasonics* **44** 259
[36] Teodori L, Costa A, Marzio R, Perniconi B, Coletti D, Adamo S, Gupta B and Tarnok A 2014 *Front. Physiol.* **5** 00218
[37] Lemaire T, Vicari E, Neufeld E, Kuster N and Micera S 2021 *IScience* **24** 103085
[38] Demir I E, Tieftrunk E, Schorn S, Saricaoglu Ö C, Pfitzinger P L, Teller S, Wang K, Waldbaur C, Kurkowski M U, Wörmann S M, Shaw V E, Kehl T, Laschinger M, Costello E, Algül H, Friess H and Ceyhan G O 2016 *BMJ-BRIT MED. J.* **65** 1001
[39] Deborde S and Wong R J 2022 *Adv. Biol.* **6** 2200089
[40] Yuasa C, Tomita Y, Shono M, Ishimura K and Ichihara A 1993 *J. Cell. Physiol.* **156** 522
[41] Sarvazyan A, Tatarinov A and Sarvazyan N 2005 *Ultrasonics* **43** 661
[42] Wang Y, Yao J, Wu X, Wu D and Liu X 2017 *J. Appl. Phys.* **122** 094902